

Fabrication and Characterization of Highly Textured Thin Films of Undoped and Ag-Doped ZnO

A. HERZI^{a,*}, M. SEBAIS^a, B. BOUDINE^a, O. HALIMI^a, B. RAHAL^b AND L. GUERBOUS^b

^aCrystallography Laboratory, Physics Department, Faculty of Exact Sciences,

Mentouri Brothers-Constantine 1 University, Route Ain El Bey, Constantine 25000, Algeria

^bNuclear Technical Division, Nuclear Research Center of Algiers, 2 Bd., Frantz Fanon, BP 399, Algiers 16000, Algeria

(Received December 17, 2018; in final form February 9, 2019)

Undoped and Ag-doped ZnO thin films with different silver concentrations (0, 1, 3, and 7 wt%) were synthesized by sol-gel method and deposited onto glass substrate by dip-coating technique. Zinc acetate dehydrate and silver nitrate were used as starting materials. 2-Methoxyethanol and ethanolamine were used as solvent and stabilizer. Characterization by X-ray diffraction has revealed that the undoped and Ag-doped ZnO are polycrystalline, and have the wurtzite hexagonal structure with a preferred orientation along *c*-axis. The nanometric size (27–34 nm) of ZnO crystallites varies with the concentration of Ag. The surface morphology analysis, by atomic force microscopy and scanning electron microscopy, depicts a homogeneous dispersion of ZnO crystallites in the form of randomly spread wrinkles-like formation. The Raman spectroscopy confirms the Ag incorporation in the ZnO lattice. All films exhibit a transmittance greater than 75% in the visible region, and a sharp absorption band at 325 nm corresponding to the fundamental absorption edge. The room-temperature photoluminescence spectra of the prepared thin films display a strong ultraviolet band at 380 nm originated from excitons recombination, and four bands in the visible region at 430 nm (violet), 460 nm, 480 nm (blue) and 530 nm (green) from created defect levels in the band gap. These synthesized materials may be potential candidates in the manufacture of devices using short wavelengths.

DOI: [10.12693/APhysPolA.135.526](https://doi.org/10.12693/APhysPolA.135.526)

PACS/topics: ZnO, Ag, thin films, sol-gel, X-ray diffraction, photoluminescence

1. Introduction

Recently, the synthesis of nanostructured thin films based on zinc oxide has been intensively investigated. These nanostructures have been applied in lot of physics devices like light-emitting diodes [1], window materials in solar cells [2, 3], gas sensors [4, 5], and photocatalysts [6–8]. Moreover, the ZnO has a direct wide band gap energy (≈ 3.37 eV at room temperature) and a high excitonic binding energy (60 meV), which make it a suitable material for optoelectronics [9].

Various techniques have been used to prepare the ZnO thin films. These techniques include the chemical vapor deposition [10], electrochemical deposition [11], spray pyrolysis [12–14], sol-gel method [15–17]. Among the techniques mentioned above, the sol-gel process has attracted a great attention due to its excellent homogeneity, low cost, easy control of doping, and chemical composition, good reproducibility, lower crystallization temperature and large-area coating capability with high adhesion on different types of substrates [18]. It has been reported that the doping of ZnO with various metal elements such as indium (In), aluminum (Al), and gallium (Ga) improve its structural, electrical, and optical properties [19, 20]. In particular, among these ZnO-based

materials, Ag-doped ZnO thin films have been intensively studied during the last decade due to their low cost, non-toxicity, low electrical resistivity, and high optical transmittance [21, 22].

In this work, the effects of silver doping (concentration of Ag: 0, 1, 3, and 7 wt%) on the structural and optical properties of ZnO thin films were examined. It was proposed earlier that the substitution sites are more energetically favorable than the interstitial sites for the synthesis and growth of ZnO crystals [6]. So ZnO and Ag-ZnO thin films were deposited onto glass substrates by dip-coating technique. Different techniques were used to investigate the evolution of the structural and optical properties of Ag-doped ZnO thin films with increase of Ag concentration.

2. Experimental

The undoped and Ag-doped ZnO thin films were prepared by sol-gel process and deposited on glass substrates by dip-coating technique. In a typical synthesis, the zinc acetate dehydrate [$\text{Zn}(\text{CH}_3\text{CO}_2)_2 \cdot 2\text{H}_2\text{O}$, ZnAc] as Zn source, and the silver nitrate [AgNO_3] as Ag source, are used as starting materials. The molar ratios of $[\text{Ag}]/[\text{Zn}]$ were 0, 1, 3, and 7 wt%. The mixture (0.75 g) was dissolved in 2-methoxyethanol (20 ml) under vigorous magnetic stirring. The resulting solution was followed by drop wise addition of ethanolamine (0.4 ml). The obtained solution was stirred for 120 min

*corresponding author; e-mail: herzikarim@yahoo.fr

at 60°C. After this heat treatment the final solution becomes transparent and homogeneous. To obtain ZnO and Ag-ZnO thin films, the cleaned glass substrates were immersed and withdrawn from the solution at the rate of 0.8 cm/min. Before the deposition of the films, the glass substrates were rinsed in an ultrasonic bath with distilled water, ethanol, and acetone then dried at room temperature. Finally, the thin films samples thus obtained were dried at 350°C for 10 min, and annealed at 500°C for 1 h. The crystalline structure was analysed with X-ray diffraction (XRD), using a PANalytical X'Pert Pro Philips diffractometer ($\lambda_{Cu} = 1.54059 \text{ \AA}$). The Raman spectroscopy was carried out by a Bruker-Senterra spectrophotometer using an excitation wavelength of 532 nm. The morphology and the topography of films were observed by scanning electron (SEM, Philips microscope) and atomic force (AFM, A100 model of APE Research) microscopies. The optical UV-visible absorption was measured using a UV-vis spectrophotometer (JASCO V-750), and the photoluminescence spectra were recorded using an excitation wavelength of 250 nm from a Perkin-Elmer LS 50B luminescence spectrophotometer.

3. Results and discussion

3.1. X-ray diffraction analysis

The XRD patterns of undoped and Ag-doped ZnO thin films, with different Ag concentrations (1, 3, and 7 wt%), deposited onto glass substrates, are presented in Fig. 1.

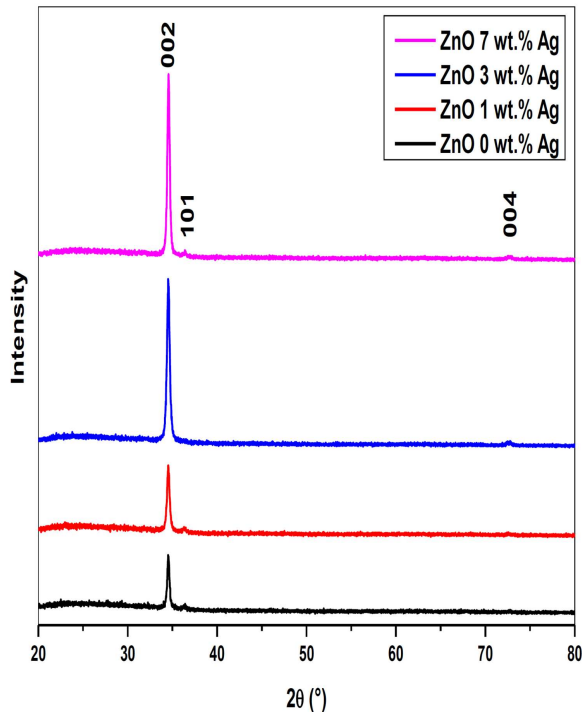


Fig. 1. X-ray diffraction diffractograms of undoped and Ag-doped ZnO thin films with different Ag concentrations (1, 3, and 7 wt%).

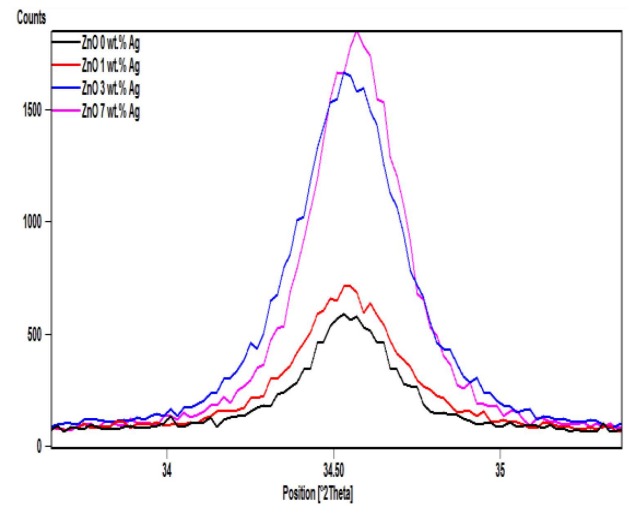


Fig. 2. Evolution of the (002) peak intensity of undoped and Ag-doped ZnO thin films with different Ag concentrations (1, 3, and 7 wt%).

The spectra show that all films are polycrystalline, and are highly textured since they exhibit a very intense peak at $2\theta = 34.52^\circ$ and a very weak peak at $2\theta = 72.58^\circ$, which correspond, to the plane (002) and its harmonic (004) of hexagonal (wurtzite) structure of ZnO, according to the JCPDS card file No. 00-36-1451 [23]. This result indicates a high preferential c -axis orientation of ZnO crystallites [24–27]. The third peak observed at $2\theta = 36.35^\circ$ is also very weak and it is from the plane (101). As for earlier synthesis [28], there are no other detected peaks corresponding to secondary phases.

From Fig. 2, we can note that the intensity of (002) peak increases with increase of the Ag concentration, and so we can conclude that the crystallinity of the films is improved by the Ag doping.

The crystallite size of undoped and Ag-doped ZnO thin films were estimated using Scherrer's formula [29, 30]:

$$D = \frac{0.9\lambda}{\beta \cos \theta} \quad (1)$$

where D is the crystallite size, λ is the wavelength, θ is the Bragg angle, and β is the full width at half-maximum (FWHM) of the peak.

On the other hand, the ZnO lattice strain σ [GPa] were calculated using the following relations [31]:

$$c_{33}^{\text{film}} = \frac{0.99c_{33}^{\text{crystal}}}{(1 - e_{zz})^4}, \quad (2)$$

$$\sigma = \left[2c_{13} - \frac{(c_{11} + c_{12})c_{33}^{\text{film}}}{c_{13}} \right] e_{zz}, \quad (3)$$

$$e_{zz} = \frac{c_0 - c}{c_0}, \quad (4)$$

where C_{ij} are the elastic constants of ZnO admit the following values: $c_{11} = 209.7 \text{ GPa}$, $c_{12} = 121.1 \text{ GPa}$, $c_{13} = 105.1 \text{ GPa}$, $c_{33} = 210.9 \text{ GPa}$ and $c_0 = 5.20661 \text{ \AA}$. C is the calculated ZnO lattice parameter along [002] axis.

TABLE I

The crystallite size values, the strains and parameters of the lattice of undoped and Ag-doped ZnO thin films (data from (002) peak).

Ag [wt%]	2θ [°]	D [nm]	a [Å]	c [Å]	e_{ZZ} $\times 10^{-4}$	c_{33}^{film}	σ^* (-) [GPa]
0	34.52	34	3.244	5.192	28	211.146	1.272
1	34.51	29	3.248	5.206	12	209.796	0.540
3	34.52	27	3.241	5.206	12	209.796	0.540
7	34.54	33	3.235	5.201	11	209.712	0.495

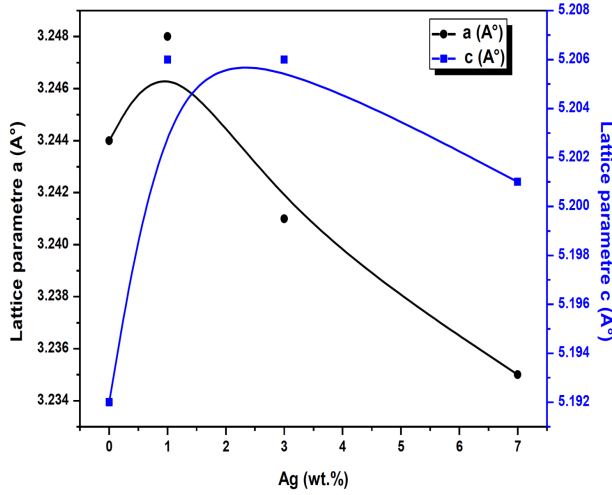


Fig. 3. Evolution of the cell parameters a [Å] and c [Å] of ZnO thin films with different Ag concentrations (0, 1, 3, and 7 wt%).

The cell parameters are calculated using the relations

$$d_{hkl} = \frac{1}{\sqrt{\frac{4}{3} \left(\frac{h^2 + k^2 + hk}{a^2} \right) + \frac{l^2}{c^2}}} \Rightarrow c = 2d_{002}, \quad (5)$$

$$a = \sqrt{\frac{4}{3} \left(\frac{h^2 + k^2 + hk}{\frac{1}{d_{hkl}^2} - \frac{l^2}{c^2}} \right)}. \quad (6)$$

The results of the average size of ZnO crystallites, the lattice strain and the cell parameters are reported in Table I.

The evolution of cell parameters, according to the percentage of Ag (0, 1, 3, and 7 wt%), are shown in Fig. 3. We note that the parameters a and c increase for the low percentages and decrease for the high percentages of Ag. This result is confirmed by the shift of the peak (002) towards the smaller and larger angles. This change in the cell parameters has, necessarily, repercussions on the optical properties of the prepared ZnO thin films.

3.2. Raman analysis

Figure 4 displays the Raman spectra of undoped and Ag-doped ZnO thin films with different Ag concentrations (0, 1, 3, and 7 wt%). The spectra exhibit compressive stress due to the substitution of Zn^{2+} (radius 0.74 Å)

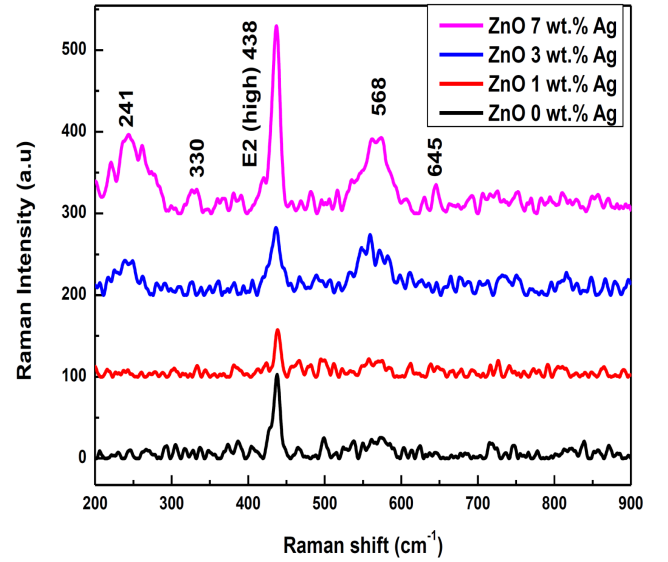


Fig. 4. Raman spectra of undoped and Ag-doped ZnO with different Ag concentrations (1, 3, and 7 wt%).

by Ag^{2+} (radius 0.89 Å) in ZnO lattice. The intense peak, situated at 438 cm^{-1} was assigned to the vibrational modes E2 (high) [32, 33], its intensity increases when Ag concentration increases, which indicates that the crystal quality of ZnO nanoparticles was improved, and ZnO crystallites have a high preferential c -axis orientation. In addition to the E2 (high) phonon mode, the intensity of the A1 (LO) mode, at 568 cm^{-1} , increases with increasing percentage of Ag. The A1(LO) was attributed to defects such as oxygen vacancies, interstitial Zn in ZnO [34, 35] or/and probably to the mode frequencies of glass substrate [33].

While the peaks at 330 and 645 cm^{-1} are from multi-phonon modes [36], the smaller peak originating at 330 cm^{-1} is attributed to a $E_{2H}-E_{2L}$ (multi-phonon) [7] and for 645 cm^{-1} c peak can also be attributed to the aggregates of Ag element doping with the start of its supersaturation [37]. Therefore, we can say that these two peaks of ZnO modes confirmed the results of XRD analysis. Moreover, the increase of Ag doping concentration up to 7 wt% leads to ameliorate the crystallization of ZnO phase. This is clearly observed by the increase of the intensity and the width of (002) intense peak in our diffractograms (Figs. 1 and 2). We observed also a supplementary peak at about 241 cm^{-1} in the Raman spectra of Ag-doped ZnO with 3 and 7 wt% of Ag doping. Mosquera et al. have attributed similar peak to the local vibrational modes (LVMS). Indeed, the incorporation of Ag in the host lattice can introduce additional modes (LVMS) in the Raman spectra [32, 38].

3.3. Surface morphology analysis

The morphology of undoped and Ag-doped ZnO thin films was analysed by SEM. From Fig. 5, one can see that the surfaces of all films exhibit a wrinkles-like morphology.

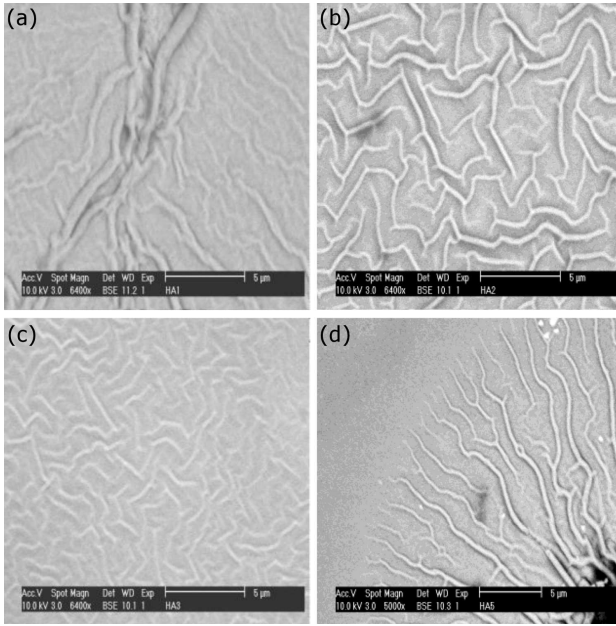


Fig. 5. SEM micrographs of ZnO thin films: (a) undoped ZnO, (b) ZnO doped with 1 wt% Ag, (c) ZnO doped with 3 wt% Ag, and (d) ZnO doped with 7 wt% Ag.

The wrinkles-like formations are interconnected with each other, and do not have a particular orientation. Their length exceeds $10 \mu\text{m}$. The wrinkles-like formations are thinner in the case of ZnO thin film doped with 3 wt% Ag. This morphology is similar to that observed by Rahal et al. [29] and Zegadi et al. [39], for ZnO thin films prepared by colloidal and sol-gel synthesis methods, respectively.

3.4. Surface topography analysis

Figure 6 shows the three-dimensional images of AFM of prepared ZnO thin films. We note that the distribution of ZnO particles on the surface of samples is uniform and the grain size is more important for the sample ZnO doped with 3 wt% Ag. The roughness increases with the concentration of Ag doping and the films exhibit a weak variation of roughness [37]. Therefore, the Ag doping affects the surface topography of films [40] and consequently can affect the optical properties.

TABLE II

Roughness by AFM of undoped and Ag-doped ZnO thin films with different Ag concentrations (1, 3, and 7 wt%).

Ag [wt%]	R_a [nm]	R_{RMS} [nm]	E_g [eV]
0	0.24	0.30	3.30
1	0.26	0.33	3.29
3	0.36	0.54	3.27
7	0.32	0.42	3.26

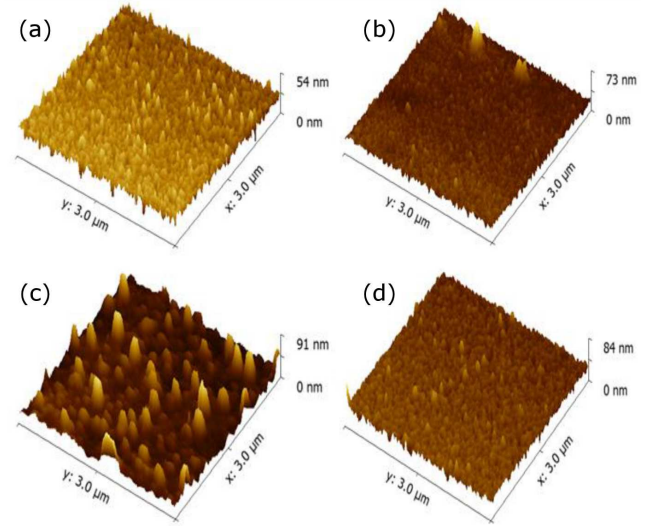


Fig. 6. AFM topography images of undoped and Ag-doped ZnO thin films with different Ag concentrations (1, 3, and 7 wt.%).

The calculated average roughness (R_a) and the root-mean square (RMS) roughness (R_{RMS}) are reported in Table II.

3.5. Optical analysis

Figure 7 displays the room temperature transmission spectra of undoped and Ag-doped ZnO thin films in the wavelength range of 200–900 nm. We can see that the optical transmittance in the visible range is greater than 75% and the samples display a cut-off wavelength at around 375 nm.

The band gap energy (E_g) of all films (undoped and Ag-doped ZnO) has been determined using the Tauc method (Fig. 8). The values of E_g are summarized in Table I. The values (3.30–3.26 eV) are close to the band gap energy of the pure ZnO ($E_g = 3.37 \text{ eV}$) [41, 42].

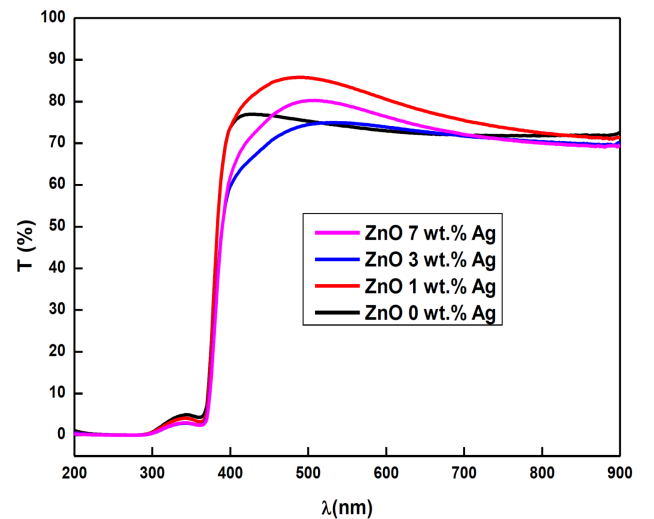


Fig. 7. Transmittance of ZnO and Ag-doped ZnO thin films.

The optical absorption edge exhibits a red-shift with the rise of Ag doping concentration. The observed band gap narrowing is due to the existence of Ag impurities in the ZnO cells, which is in agreement with literature [24, 25, 43].

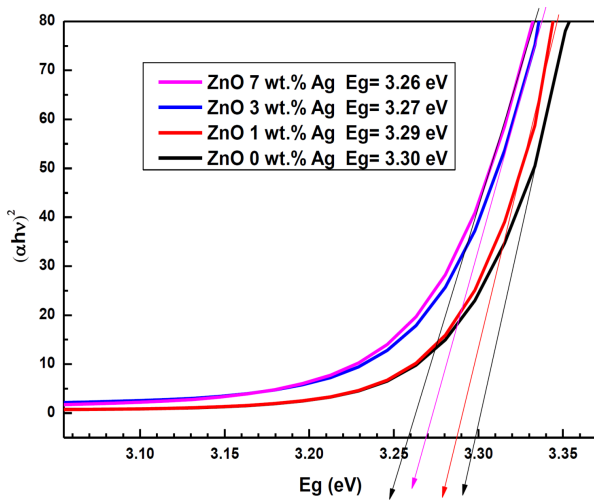


Fig. 8. Determination of the band gap energy of ZnO and Ag-doped ZnO thin films.

3.6. Photoluminescence analysis

Figure 9 exhibits the room temperature photoluminescence spectra (excitation wavelength 325 nm) of undoped and Ag-doped ZnO thin films.

We remark that the PL signal is formed by five broadened bands. In order to determine the center of every luminescence band, the signal has been deconvoluted with the Gauss curve (Fig. 10).

Thus, the bands were located at 2.34 eV (530 nm), 2.58 eV (480 nm), 2.70 eV (460 nm), 2.88 eV (430 nm) and 3.26 eV (380 nm). The band at 3.26 eV can be attributed to the exciton recombination corresponding to

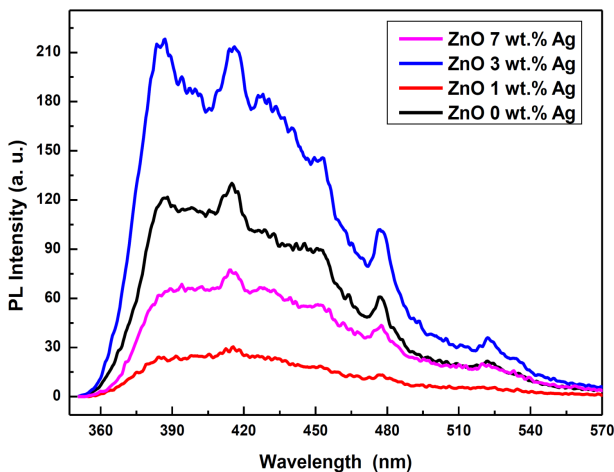


Fig. 9. Photoluminescence spectra of undoped ZnO and Ag-doped ZnO thin films with different Ag concentrations (1, 3, and 7 wt%).

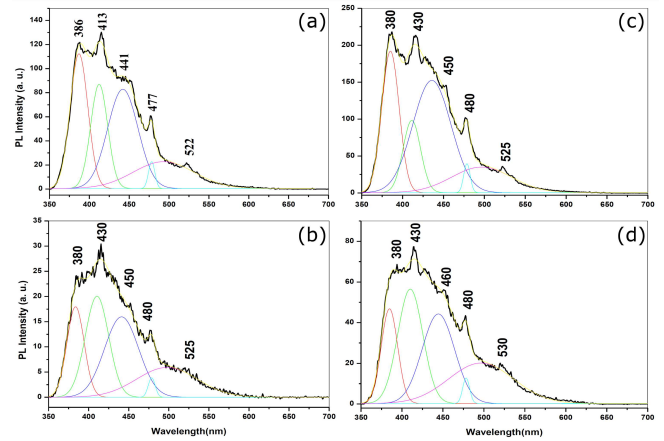


Fig. 10. Deconvolution of photoluminescence spectra of undoped and Ag-doped ZnO thin films with different Ag concentrations (1, 3, and 7 wt%).

the near-band edge transition (NBE) of ZnO [44]. The band observed at 2.88 eV may be assigned to the transition energy of electron from conduction band to the zinc vacancy V_{Zn} [45]. The bands at 2.70 eV and 2.58 eV are originated from interstitial zinc Zn_i and oxygen defects [46, 47]. The band situated at 2.34 eV can be assigned to intrinsic defects (oxygen vacancies, zinc interstitials, O interstitials, or anti-site defects) [48]. These emission bands are possible because they arise from levels of different energies created in the forbidden band. The position of the bands changes slightly with the concentration of the Ag doping (Figs. 9 and 10) and the ZnO thin film doped with 3 wt% Ag displays the most intense luminescence bands.

4. Conclusion

Undoped and Ag-doped ZnO thin films were synthesized by sol-gel method and deposited onto glass substrate by dip-coating technique. Their structural, morphological and optical properties have been studied. The X-ray diffraction showed that the thin films are polycrystalline and crystallized in hexagonal (wurtzite) structure with a preferential orientation of crystallites along c axis. The crystallites have nanometric sizes. This result has been confirmed by the Raman, the SEM and the AFM investigations. The optical characterization has demonstrated that the prepared ZnO and Ag-doped ZnO thin films are highly transparent in the visible domain. The energy of the optical band gap decreases from 3.30 to 3.26 eV when Ag doping increases, and the photoluminescence spectra of films show an emission band in the ultraviolet (380 nm) and four bands in the visible region. The ZnO thin film with 3 wt% Ag doping gave the most intense luminescence bands.

References

- [1] R. Könenkamp, R.C. Word, M. Godinez, *Nano Lett.* **5**, 2005 (2005).
- [2] L.C. Claude, T.Z. Ramon, M.A. Ryan, *Adv. Mater.* **17**, 1512 (2005).

- [3] B. Mereu, O. Caglar, J.S. Cashmore, P.A. Losio, A. Salabas, I. Sinicco, *Sol. Energy Mater. Sol. Cells* **152**, 147 (2016).
- [4] H.J. Lim, D. Yong, Y.J. Oha, *Sens. Actuat. A* **125**, 405 (2006).
- [5] M. Miki-Yoshida, V. Collins-Martínez, P. Amezaga-Madrid, P.A. Aguilar-Elguezabal, *Thin Solid Films* **419**, 60 (2002).
- [6] S.M. Hosseini, I.A. Sarsari, P. Kameli, H. Salamati, *J. Alloys Comp.* **640**, 408 (2015).
- [7] R. Kumar, D. Rana, A. Umar, P. Sharma, S. Chauhan, M.S. Chauhan, *Talanta* **137**, 204 (2015).
- [8] O. Bechambi, M. Chalbi, W. Najjar, S. Sayadi, *Appl. Surf. Sci.* **347**, 414 (2015).
- [9] A. Baltakesmez, S. Tekmen, S. Tuzemen, *J. Appl. Phys.* **110**, 054502-7 (2011).
- [10] S. Fay, U. Kroll, C. Bucher, E. Vallat-Sauvain, A. Shah, *Sol. Energy Mater. Sol. Cells* **86**, 385 (2005).
- [11] M. Harati, D. Love, W.M. Lau, Z. Ding, *Mater. Lett.* **89**, 339 (2012).
- [12] H. Belkhalifa, H. Ayed, A. Hafdallah, M.S. Aida, R.T. Ighil, *Optik* **127**, 2336 (2016).
- [13] A. Gahtar, A. Rahal, B. Benhaoua, S. Benramache, *Optik* **125**, 3674 (2014).
- [14] M. Tomakin, *Superlatt. Microstruct.* **51**, 372 (2012).
- [15] T. Jannane, M. Manoua, A. Liba, N. Fazouan, A. El Hichou, A. Almaggoussi, A. Outzourhit, M. Chaik, *J. Mater. Environ. Sci.* **8**, 160 (2017).
- [16] F. Xian, K. Miao, X. Bai, Y. Ji, F. Chen, X. Li, *Optik* **124**, 4876 (2013).
- [17] F. Khan, S.-H. Baek, J.H. Kim, *J. Alloys Comp.* **584**, 190 (2014).
- [18] K. Necib, T. Touam, A. Chelouche, L. Ouarez, D. Djouadi, B. Boudine, *J. Alloys Comp.* **735**, 2236 (2018).
- [19] X. Du, J. Li, X. Bi, *J. Alloys Comp.* **698**, 128 (2017).
- [20] C. Lung, M. Toma, M. Pop, D. Marconi, A. Pop, *J. Alloys Comp.* **725**, 1238 (2017).
- [21] N. Srinatha, Y.S. No, V.B. Kamble, S. Chakravarty, N. Suriyamurthy, B. Angadi, A.M. Umarji, W.K. Choi, *RSC Adv.* **6**, 9779 (2016).
- [22] E. Fortunato, D. Ginley, H. Hosono, D.C. Paine, *MRS Bull.* **32**, 242 (2007).
- [23] Joint Committee for Powder Diffraction Standards, *Power Diffraction File for Inorganic Materials*, JCPDS 1979, p. 79.
- [24] A. Arunachalam, S. Dhanapandian, M. Rajasekaran, *J. Anal. Appl. Pyrol.* **123**, 107 (2017).
- [25] M. Dehimi, T. Touam, A. Chelouche, F. Boudjouan, D. Djouadi, J. Solard, A. Fischer, A. Boudrioua, A. Doghmane, *Adv. Condens. Matter Phys.* **2015**, 740208 (2015).
- [26] R. Jayakrishnan, K. Mohanachandran, R. Sreekumar, C.S. Kartha, K.P. Vijayakumar, *Mater. Sci. Semicond. Process.* **16**, 326 (2013).
- [27] Y. Liu, J. Lian, *Appl. Surf. Sci.* **253**, 3727 (2007).
- [28] L. Castañeda, A. Maldonado, A. Escobedo-Morales, M. Avendano-Aleso, H. Gómez, J. Vega-Pérez, M.L. Olvera, *Mater. Sci. Semicond. Process.* **14**, 114 (2011).
- [29] B. Rahal, B. Boudine, A.R. Khantoul, M. Sebais, O. Halimi, *Optik* **127**, 6943 (2016).
- [30] H. Benelmadjat, N. Touka, B. Harieche, B. Boudine, O. Halimi, M. Sebais, *Opt. Mater.* **32**, 764 (2010).
- [31] H. Benelmadjat, S. Boudjaadar, B. Boudine, A. Chelouche, O. Halimi, A. Boudrioua, *J. Optoelectron. Adv. Mater.* **13**, 122 (2011).
- [32] A.H. Shah, E. Manikandan, M.B. Ahmed, V. Ganesan, *J. Nanomed. Nanotechnol.* **4**, 168 (2013).
- [33] A. Khan, *J. Pak. Mater. Soc.* **4**, 5 (2010).
- [34] L.N. Wang, L.Z. Hu, H.Q. Zhang, Y. Qiu, Y. Lang, G.Q. Liu, J.Y. Ji, J.X. Ma, Z.W. Zhao, *Mater. Sci. Semicond. Process.* **14**, 274 (2011).
- [35] W.J. Li, C.Y. Kong, H.B. Ruan, G.P. Qin, G.J. Huang, T.Y. Yang, W.W. Liang, Y.H. Zhao, X.D. Meng, P. Yu, Y.T. Cui, L. Fang, *Solid State Commun.* **152**, 147 (2012).
- [36] B. Hadžić, N. Romčević, D. Sibera, U. Narkiewicz, I. Kuryliszyn-Kudelska, W. Dobrowolski, M. Romčević, *J. Phys. Chem. Solids* **91**, 80 (2016).
- [37] Q.T.H. Ta, S. Park, J.S. Noh, *J. Coll. Interface Sci.* **505**, 437 (2017).
- [38] E. Mosquera, C. Rojas-Michea, M. Morel, F. Gracia, V. Fuenzalida, R.A. Zárate, *Appl. Surf. Sci.* **347**, 561 (2015).
- [39] C. Zegadi, K. Abdelkebir, D. Chaumont, M. Adnane, S. Hamzaoui, *Adv. Mater. Phys. Chem.* **4**, 93 (2014).
- [40] F. Xian, K. Miao, X. Bai, Y. Ji, F. Chen, X. Li, *Optik* **124**, 4876 (2013).
- [41] D. Basak, G. Amin, B. Mallik, G.K. Paul, S.K. Sen, *J. Cryst. Growth* **256**, 73 (2003).
- [42] S.J. Pearton, D.P. Norton, K. Ip, Y.W. Heo, T. Steiner, *J. Vac. Sci. Technol. B* **22**, 932 (2004).
- [43] A. Chelouche, D. Djouadi, H. Merzouk, A. Aksas, *Appl. Phys. A* **115**, 613 (2014).
- [44] P. Li, S. Wang, J. Li, Y. Wei, *J. Lumin.* **132**, 220 (2012).
- [45] X.R. Deng, H. Deng, M. Wei, J.J. Chen, *J. Mater. Sci. Mater. Electron.* **23**, 413 (2012).
- [46] K. Rokesh, A. Pandikumar, K. Jothivenkatachalam, *Mater. Focus* **3**, 345 (2014).
- [47] K. Rokesh, S.C. Mohan, S. Karuppuchamy, K. Jothivenkatachalam, *J. Environm. Chem. Eng.* **6**, 3610 (2017).
- [48] K. Xianwen, S. Fukai, S.P. Young, W. Yunjin, W.K. Tae, F. Dejun, *Surf. Coat. Technol.* **201**, 6797 (2007).